AIAA 2001-1279

Analyses for Debonding of Stitched Composite Sandwich Structures Using Improved Constitutive Models

E.H. Glaessgen, D.W. Sleight,
T. Krishnamurthy and I.S. Raju
NASA Langley Research Center
Hampton, VA 23681

42nd AIAA/ASME/ASCE/AHS/ASC
Structures, Structural Dynamics, and
Materials Conference
April 16-19, 2001/Seattle, WA

AIAA-2001-1279

ANALYSES FOR DEBONDING OF STITCHED COMPOSITE SANDWICH STRUCTURES USING IMPROVED CONSTITUTIVE MODELS

E.H. Glaessgen*, D.W. Sleight*, T. Krishnamurthy** and I.S. Raju†
NASA Langley Research Center, Hampton, VA 23681-0001, U.S.A.

Abstract

A fracture mechanics analysis based on strain energy release rates is used to study the effect of stitching in debonded sandwich beam configurations. Finite elements are used to model the configurations. The stitches were modeled as discrete nonlinear spring elements with a compliance determined by experiment. The constitutive models were developed using the results of flatwise tension tests from sandwich material rather than monolithic material. The analyses show that increasing stitch stiffness, stitch density and debond length decrease strain energy release rates for a fixed applied load.

Introduction

Composite sandwich construction is very attractive for use in aerospace structures (Figure 1). Composite sandwich structures are more cost effective to manufacture than traditional skin-stringer structures and have better fatigue resistance. Recent studies show that sandwich structure has the potential to be the lightest and lowest cost manufacturing concept for fuselage structure [1]. While these configurations are efficient, sandwich panels can be easily damaged by foreign object impacts. This critical deficiency has prevented the use of sandwich construction in most primary aerospace structures.

Debonds along the skin-core interfaces are considered limiting to a sandwich structure since the skin is free to "peel away" from the core resulting in catastrophic failure. This limitation is enough to discourage most aerospace manufacturers from using sandwich construction in primary structures. To overcome these limitations a method of mechanically fastening the skin to the core is needed. This method must be inexpensive and should not add a significant amount of weight to the sandwich structure.

Stitching the skin and core is proposed here as a joining methodology. Stitched warp-knit textile composite materials are currently being considered for use in primary aerospace structures and as facesheets for sandwich structures. Structures manufactured from these materials offer advantages in manufacturability and damage tolerance over conventional composite and metallic structures. Manufacturability is improved because large sections of dry carbon textile preform and core can be assembled and stitched with Kevlar threads near net shape before the epoxy resin is introduced.[2] Improvements in damage tolerance are observed because the Kevlar stitches tend to prevent propagation of debonds and delaminations that may be caused by in-plane and out-of-plane loadings.

Figure 1 shows a representative section of composite sandwich structure where stitches, in addition to the resin interface, are used to attach the facesheets to the core. This structure may be subjected to a variety of loads as shown in the figure. Figure 2 shows a simplified configuration that may be used to gain insight into the behavior of more complex configurations.

The objective of this paper is to study the effect of stitches on the response of a sandwich debond configuration. The parameters studied are the effects of stitch stiffness and stitching density, core stiffness and debond length. New constitutive models for the stitches have been determined from flatwise tensile tests of a sandwich material and are implemented in the present analyses. A debond between the top face sheet and the core is assumed and strain energy release rates at the debond front are used to evaluate the effects of several parameters using finite element analyses and the virtual crack closure technique (VCCT).

Debonded Sandwich Beam Configuration

A debonded sandwich beam configuration subjected to tensile loading is shown in Figure 2(b). The stitched sandwich beam structure is assumed to have Kevlar stitches, foam core, and carbon facesheets as shown in the figure. The parameters of this configuration are the length of the specimen, L, the thickness of the facesheets, t_f, the thickness of the core, t_c, and the spacing of the stitches, s. The local details of a debond of length, a, propagating from one end of the configuration including the loading of the stitches are shown in the figure.

* Aerospace Engineer, Analytical and Computational Methods Branch, Member AIAA
** Aerospace Engineer, Analytical and Computational Methods Branch, Senior Member AIAA
† Head, Analytical and Computational Methods Branch, Associate Fellow AIAA

Facesheet material and thicknesses that are representative of a hybrid IM7/3501-6 and AS4/3501-6 warp-knit fabric are considered.[3] The material consists of IM7 yarns in the axial direction and AS4 yarns in the off-axis directions. Each stack of material is assumed to be oriented with its primary axis in the x-direction and having a thickness of 0.055 in. The overall density of the fabric expressed in areal weight is 0.577 oz./ft.^{2}, 1.21 oz./ft.^{2} and 0.651 oz./ft.^{2} for the forty-five, zero and ninety degree plies, respectively. The equivalent laminate stacking sequence of each stack of material is $(45/\text{-}45/0/90/0/\text{-}45/45)_{ns}$ where n=2 for both of the facesheets.

Finite Element Analysis

Figure 1 shows a stitched sandwich shell-type structure. Three-dimensional modeling and analysis of this complex configuration requires a large finite element model. However, considerable insight into the behavior of such a complicated configuration can be obtained by studying simpler configurations such as the debonded sandwich beam configuration shown in Figure 2 while reducing modeling complexity. The debonded sandwich beam configuration was modeled using the ABAQUS finite element code.[4]

The method of analysis implemented here involves the use of plane strain continuum elements to model the configuration and nonlinear spring elements with experimentally determined compliances to model the stitches. This modeling technique allows an experimentally determined load vs. deflection behavior to be considered for each stitch. The stitch response includes the local effects of the stitch debonding from the laminate in addition to nonlinearity of the laminate, core and stitch materials.[5]

The specimen configurational parameters including facesheet and core thicknesses and stitch spacing are shown in Figure 2(a) and Table 1. Debond lengths, a, between 0.250 in. (a/t_f=2.27) and 2.00 in. (a/t_f=18.2) are considered for the unstitched and stitched configurations with a length, L=7.00 in. and an applied load, P=100 lb.

Material Properties

In these analyses, the laminates are assumed to be homogeneous with axial properties determined experimentally and all others estimated using the equivalent stacking sequence and classical lamination theory as

E_{11}=11.7 *Msi* μ_{12}=2.50 *Msi* υ_{12}=0.40
E_{22}=5.14 *Msi* μ_{13}=1.77 *Msi* υ_{13}=0.30
E_{33}=1.79 *Msi* μ_{23}=0.88 *Msi* υ_{23}=0.30

where E_{ii}, μ_{ij}, υ_{ij} (i,j=1,2,3) are the Young's moduli, shear moduli, and Poisson's ratio, respectively, and the subscripts 1,2,3 represent the fiber, transverse and out-of-plane directions, respectively.

Three cases of core properties are considered. The first two cases consider a foam core approximated as an isotropic continuum with elastic properties (E_c, ν) and densities (ρ) taken from vendor data as

E_c^1=5220 *psi* υ^1=0.385 ρ^1=2.0 *lb./ft.*^{3}
E_c^2=13340 *psi* υ^2=0.385 ρ^2=4.68 *lb./ft.*^{3}

The third case considers a core with the same orthotropic properties as the facesheets ($E_c^3=E_{facesheets}$). Core moduli and stitch spacings for all of the debonded sandwich beam configurations considered in this paper are shown in Table 1. The three cases represent soft and medium density foam cores and the extreme case of a core having the same properties as the carbon/epoxy facesheets.

Strain Energy Release Rates

The configuration was modeled with the ABAQUS finite element code using 8-noded quadratic two-dimensional (plane strain) elements.[4] A representation of the 8-noded plane strain elements near a debond front with rectangular grid type modeling is shown in Figure 3 with elements having length of 0.0625 in. The elements are assumed to have the same length, Δ, ahead of and behind the debond front (as shown in Figure 3(b)). The G-values can be calculated using the nodal forces (F_x, F_z) and displacements (u, w) near the debond front and the increment of new debond area created using the VCCT as (see Figure 3)[6,7]

Mode-I components:

$$G_I = -\frac{1}{2\Delta}\left[F_{z_i}\left(w_p - w_{p'}\right) + F_{z_j}\left(w_l - w_{l'}\right)\right] \tag{1}$$

Mode-II components:

$$G_{II} = -\frac{1}{2\Delta}\left[F_{x_i}\left(u_p - u_{p'}\right) + F_{x_j}\left(u_l - u_{l'}\right)\right] \tag{2}$$

with

$$G_{Total} = G_I + G_{II}. \tag{3}$$

Table 1: Configurations

Configuration	Facesheet Thickness t_f (in.)	Core Thickness t_c (in.)	Stitch Spacing s (in.)	First Stitch Location (in.)	Core Modulus E_c (psi)
N-1	0.110	0.500	N/A	N/A	5220
N-2	0.110	0.500	N/A	N/A	13340
N-3	0.110	0.500	N/A	N/A	$E_{ij}^{core} = E_{ij}^{facesheets}$
S4-1	0.110	0.500	0.250	0.00	5220
S4-2	0.110	0.500	0.250	0.00	13340
S4-3	0.110	0.500	0.250	0.00	$E_{ij}^{core} = E_{ij}^{facesheets}$
S2-1	0.110	0.500	0.500	0.00	5220
S2-2	0.110	0.500	0.500	0.00	13340
S2-3	0.110	0.500	0.500	0.00	$E_{ij}^{core} = E_{ij}^{facesheets}$
S41-1	0.110	0.500	0.250	0.250	5220
S41-2	0.110	0.500	0.250	0.250	13340
S41-3	0.110	0.500	0.250	0.250	$E_{ij}^{core} = E_{ij}^{facesheets}$
S21-1	0.110	0.500	0.500	0.500	5220
S21-2	0.110	0.500	0.500	0.500	13340
S21-3	0.110	0.500	0.500	0.500	$E_{ij}^{core} = E_{ij}^{facesheets}$

The strain energy release rates of the debonded sandwich beam configurations are calculated using equations (1)-(3) with the nodal forces and displacements transformed into a coordinate system that is normal to the debond front in a geometrically nonlinear analysis. For cases with a stitch present at the debond front nodal location, the stitch force is subtracted from the computed force at the debond front in the VCCT calculations consistent with the calculations in reference 7 for pressure loaded debond faces.

This configuration may exhibit an oscillatory stress field very near the debond front and demonstrates nonconvergence of the individual modes of the strain energy release rate. The computed values of G_I and G_{II} do not converge with decreasing element size, however, the sum of the modes does converge and is given as G_{Total} in Eq. (3).[7,8]

Modeling Stitches

The configurations have been analyzed with a geometrically nonlinear finite element analysis within the ABAQUS finite element code. Using similar techniques discussed in references (9-11), the stitches are modeled as nonlinear spring elements rather than as spar or beam elements.

The spring elements are assumed to have only axial stiffness, K_{axial}. Unlike the analyses discussed in references (9-11), spring elements ahead of and behind the debond front are considered because of the through-the-thickness deformation of the compliant foam core. The nonlinear spring elements are evenly spaced along the debonded length of the model. The stitch location spacing presented in Table 1 coincides with element corner nodal locations.

Compliance curves for both axial and shear behavior of the stitches embedded within a laminated carbon/epoxy textile composite with material properties similar to those of the sandwich facesheets were developed in reference 5 using flatwise tension and double lap shear tests. Similar curves have been developed for a Kevlar stitch embedded within a sandwich material. Constitutive behavior of the stitch was determined from flatwise tensile tests of a sandwich composite with a Teflon insert separating the facesheets from the core, thus allowing the nonlinear response of the stitches to be determined.

Two flatwise tensile specimens were tested and curves representing their load-deflection behavior (stiffness) are labeled as *Specimen 1* and *Specimen 2* in Figure 4. A curve representing the average load-deflection behavior of the two specimens along with curves representing hypothetical upper and lower bounds are also shown in the figure. The upper and lower bounds on likely stitch stiffnesses are assumed to be 150% (stiff stitch values) and 50% (compliant stitch values) of the average stiffness, respectively. These compliance curves represent the net behavior of the stitch due to stitch, core and facesheet material nonlinearity and stitch debonding.[5]

A piecewise linear representation of this data is used in the finite element model. Examination of the flatwise tensile test data revealed that the axial stiffness of the stitches increases from approximately 3300 lb./in. initially to 5500 lb./in. near failure. Note that failure of the stitches occurs at an average load of 60 lb. per stitch. These stiffnesses and failure loads are used for the characterizations in this paper.

Each stitch is modeled with a single nonlinear spring element joining the inner surfaces of the upper and lower facesheets. Thus, compatibility between the

stitches and core is not maintained, nor is contact between the stitches and the core considered. The effect of this simplification may be minor when considering compliant cores, but should become more important as the stiffness of the core increases.

Modeling the Facesheet to Core Contact Problem
Closure of the debonded faces may occur once the debond is of sufficient length because of the stitch forces. In the finite element analysis, contact of the faces is allowed, while interpenetration of the faces is not. In references (9-11), interpenetration of the faces was prevented by adding multipoint constraints along a known region of interpenetration to impose the requirement of identical z-direction (w) displacements among elements in contact.

Because of the compliance of the core in the sandwich structure, the stitches are assumed to carry load in compression as well as tension. In the present analysis, the stiffness of the stitches in compression is assumed to be equal to the initial stiffness of the stitches in tension. Given this assumption, the computed values of facesheet to core interpenetration typically were less than 0.2% of the facesheet thickness. Thus, multipoint constraints are not used in the present analysis.

Results and Discussion

Four variables are considered in this analysis and include stitch stiffness, stitch configuration, core stiffness and debond length. Three stitch stiffnesses are considered: the average value from testing and 150% and 50% of the average value. Five stitch configurations are considered: (a) unstitched, (b) four stitches per inch, (c) two stitches per inch, (d) four stitches per inch with no stitch under the load, and (e) two stitches per inch with no stitch under the load. Configurations (b) and (c) have their first stitch directly beneath the load while configurations (d) and (e) have their first stitch offset from the load by a distance equal to the stitch spacing. Three core stiffnesses are considered: a compliant core with modulus, E_c^1=5220 psi; an intermediate stiffness core with modulus, E_c^2=13340 psi; and a stiff core with modulus, $E_c^3=E_{facesheets}$. Finally, debond lengths, a, between 0.250 in. (a/t_f=2.27) and 2.00 in. (a/t_f=18.2) are considered with an applied load, P, of 100 lb.

As shown in Figure 5, the unstitched configurations exhibit increasing G_{Total} with increasing debond length, a, for all three moduli (configurations *N-1*, *N-2* and *N-3* in Table 1). However, increasing core modulus decreases G_{Total} even for large debond lengths.

In the discussion of the stitched configurations shown in Figures 6 through 10, results are given for (a) stiff stitch values, (b) average stitch values and (c) compliant stitch values as shown in Figure 4.

The effect of stitching is shown in Figures 6(a) through 6(c) for configurations with four stitches per inch (*S4-1*, *S4-2* and *S4-3*). The slope of the G_{Total} curve for stitched configurations with foam core (*S4-1* and *S4-2*) decreases for all stitch stiffnesses and all debond lengths because of the load transfer of the stitches. The slope of the G_{Total} curve does not begin to decrease for the configurations with the stiffest core (*S4-3*) until the third stitch begins to carry load. The G_{Total} continues to decrease with both the number of loaded stitches and the distance from the debond front to each of the load-bearing stitches. For long debonds (a/t_f>9.09), the strain energy release rate approaches near-zero values in the stitched configurations. Note that the G-values are functions of stitch stiffness but even the compliant stitches have a profound effect on the G-values as the debond length increases.

The effect of a lower stitching density (2 stitches per inch) is shown in Figures 7(a) through 7(c). As with the *S4* configurations, the *S2* configurations (*S2-1*, *S2-2* and *S2-3*) show a general decrease in G_{Total} with increasing a/t_f. The reduction in strain energy release rate requires a longer length of debond growth because there are fewer load bearing stitches per inch of debond length. G-values are somewhat larger for the configurations with lower stitching density than for the configurations with four stitches per inch but this effect is not as significant as that of the stiffness of the individual stitches themselves (e.g. compare Figure 7(a) and 7(c)).

The effect of stitch placement is considered next. Note that a load bearing stitch is present at x=0 in. (immediately below the point of load application) in both the *S4* and *S2* configurations. Figures 8(a) through 8(c) show G_{Total} plotted against debond length for configurations with four stitches per inch and missing the stitch immediately beneath the load (*S41-1*, *S41-2* and *S41-3*). Compared with configurations *S4* (Figure 6), the maximum values of G_{Total} for configurations *S41* (Figure 8) have increased significantly. Although the effect of the stitches is delayed and somewhat reduced, the analyses for long debond lengths (a/t_f>9.09) shows that G_{Total} decreases toward zero as the debond grows even with sparse stitching.

Finally, the extreme case of two stitches per inch with no stitch under the load (*S21-1*, *S21-2* and *S21-3*) is

considered in Figures 9(a) through 9(c). Note that the maximum value on the vertical scale has increased from 2.0 in.-lb./in.^{2} to 5.0 in.-lb./in.^{2} Again, the stitches are shown to reduce the G-values to near zero for long debond lengths, (a/t_f=18.2).

The decrease in G_{Total} for longer debond lengths is the result of the stitches resisting debond opening (reducing the opening force in the region near the debond front.) This effect increases with increasing distance between the debond front and each load bearing stitch and also with increasing numbers of load bearing stitches.

Concluding Remarks

The effect of stitches on the total strain energy release rate for a debonded sandwich beam configuration with an initial debond was studied. Plane strain finite elements were used to model the configuration and the virtual crack closure technique was used to calculate the strain energy release rates. Using this fracture mechanics approach, a debond between the skin and stiffener flange was assumed. The debond growth between the facesheet and core was assumed to be self-similar and continuous along the length of the interface. The stitches were modeled as discrete nonlinear spring elements with their compliance determined by experiment. Interaction between the stitches and core was not considered.

For the unstitched configuration, G_{Total} decreases with increasing core modulus. The effect of stitching was most significant for compliant configurations. As the debond length increases, additional stitches begin to carry load resulting in a decrease in G_{Total}. For long debonds, the stitches may produce enough compressive force at the debond front to close the debond and reduce G_{Total} to near-zero values. The stitching density, stitch stiffness and proximity of the first stitch to the point of load application effect the rate at which G_{Total} decreases. Configurations with a dense stitch pattern and stiff stitches decrease G_{Total} more rapidly than configurations with sparse or compliant stitching.

References

1. Polland, D.R., Finn, S.R., Griess, K.H., Hafenrichter, J.L., Hanson, C.T., Ilcewicz, L.B., Metschan, S.L., Scholz, D.B., and Smith, P.J., "Global Cost and Weight Evaluation of Fuselage Side Panel Design Concepts," NASA CR 4730, April 1997.
2. Wang, J.T., Jegley, D.C., Bush, H.G. and Hinrichs, S.C., "Correlation of Structural Analysis and Test Results for the McDonnell Douglas Stitched/RFI All-Composite Wing Stub Box," *NASA TM-110267*, 1996.
3. Davis, J.G., Shuart, M.J. and Bowles, D.E., Eds., *Fifth NASA/DoD Advanced Composites Technology Conference*, NASA CP 3294, May 1995.
4. ABAQUS/Standard User's Manual, Version 5.8, Hibbitt, Karlsson and Sorensen, Inc., Pawtucket, RI.
5. Adams, D.O., "Stitch Compliance in Delaminated Composites," *29th SAMPE Technical Conference*, Orlando, FL, October 28-31, 1997.
6. Rybicki, E.F. and Kanninen, M.F., "A Finite Element Calculation of Stress Intensity Factors by a Modified Crack Closure Integral," *Engineering Fracture Mechanics*, Vol. 9, 1977, pp. 931-938.
7. Raju, I.S., "Calculation of Strain-Energy Release Rates with Higher Order and Singular Finite Elements," *Engineering Fracture Mechanics*, Vol. 28, No. 3, 1987, pp. 251-274.
8. Smith, S.A., Shivakumar, K.N. and Raju, I.S., "An Evaluation of Mixed-Mode Energy Release Rate in Cracked Sandwich Beam Fracture Specimen," *41st AIAA/ASME/ASCE/AHS Structures, Structural Dynamics and Materials Conference*, AIAA , 2000.
9. Glaessgen, E.H., Raju, I.S. and Poe, Jr., C.C., "Fracture Mechanics Analysis of Stitched Stiffener-Skin Debonding," *39th AIAA/ASME/ASCE/AHS Structures, Structural Dynamics and Materials Conference*, AIAA Paper 98-2022-CP, 1998.
10. Glaessgen, E.H., Raju, I.S. and Poe, Jr., C.C., "Plate Element-Based Models for Mixed-Mode Debonding of Stitched Stiffened Panels," *STP 1360, Fatigue and Fracture Mechanics: 30th Volume*, ASTM, 1998, pp. 456-472.
11. Glaessgen, E.H., Raju, I.S. and Poe, Jr., C.C., "Delamination and Stitch Failure in Stitched Composite Joints," *40th AIAA/ASME/ASCE/AHS Structures, Structural Dynamics and Materials Conference*, AIAA Paper 99-1247-CP, 1999.

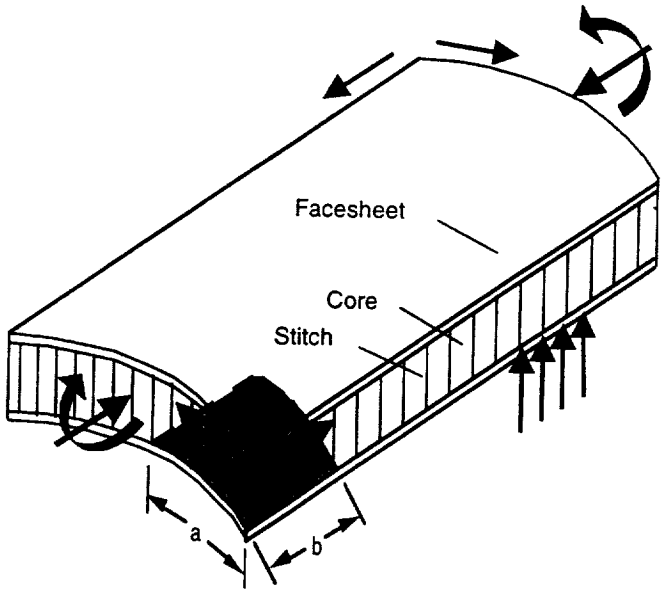

Figure 1. Stitched sandwich concept.

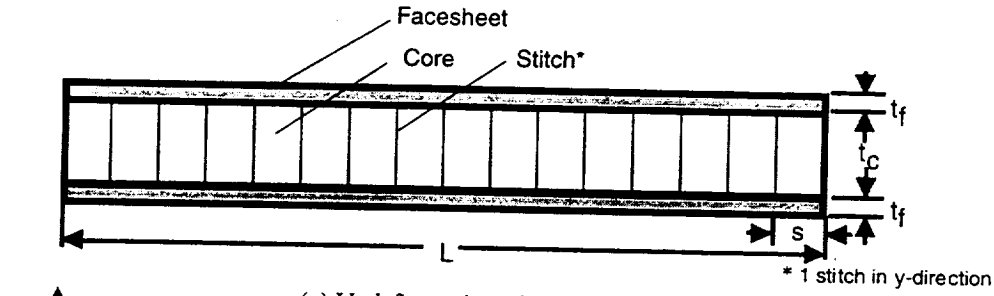

(a) Undeformed configuration

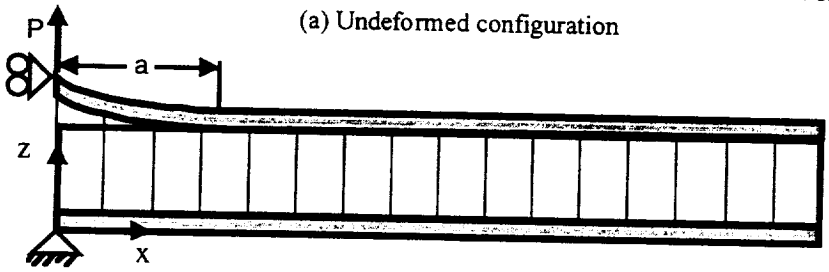

(b) Deformed configuration and boundary conditions

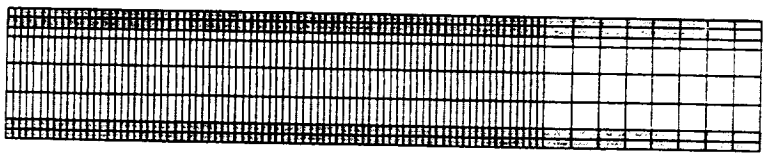

(c) Typical finite element mesh

Figure 2. Debonded sandwich beam configuration.

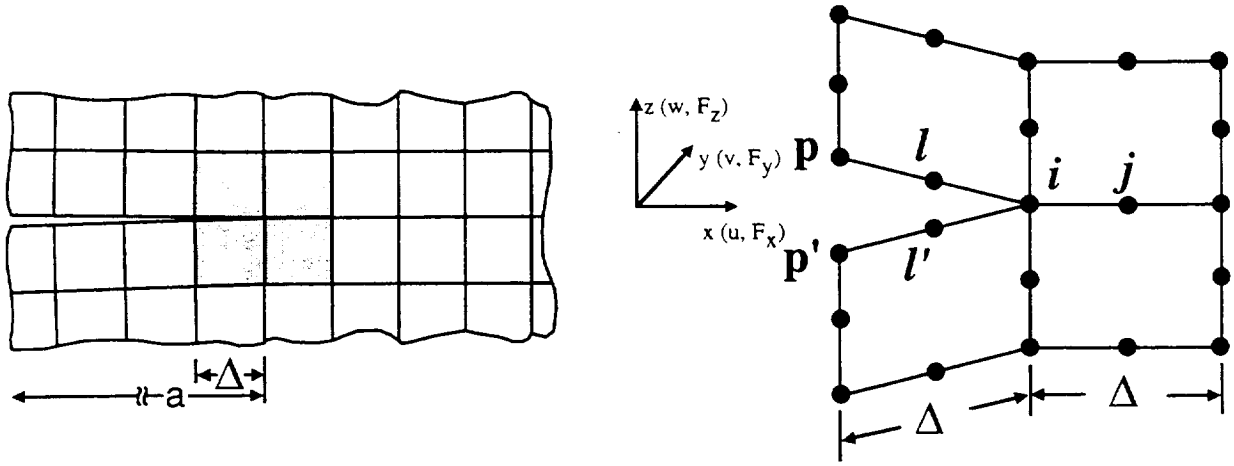

(a) Finite element modeling near the debond front

(b) Details of the model near the debond front

Figure 3. Debonded sandwich beam configuration modeled with 8-noded plane strain elements.

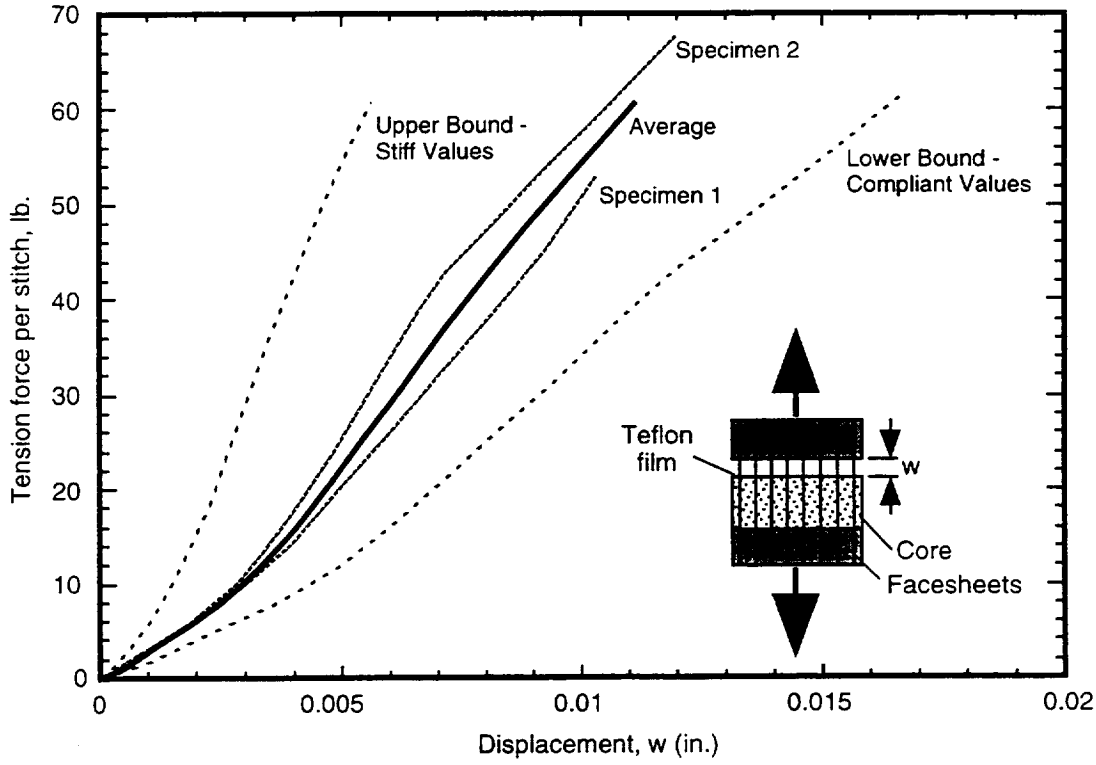

Figure 4. Stitch stiffness.

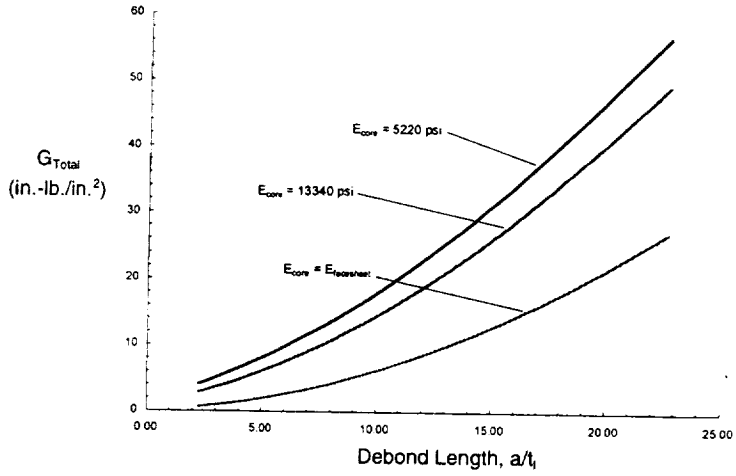

Figure 5. Strain energy release rate for unstitched configuration.

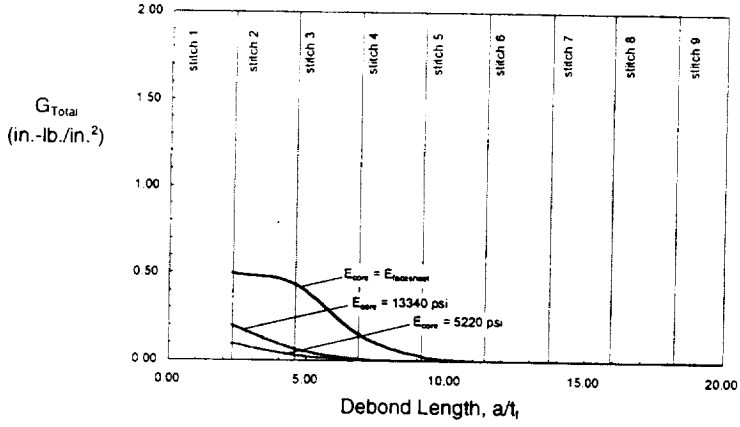

(a) Stiff stitch values

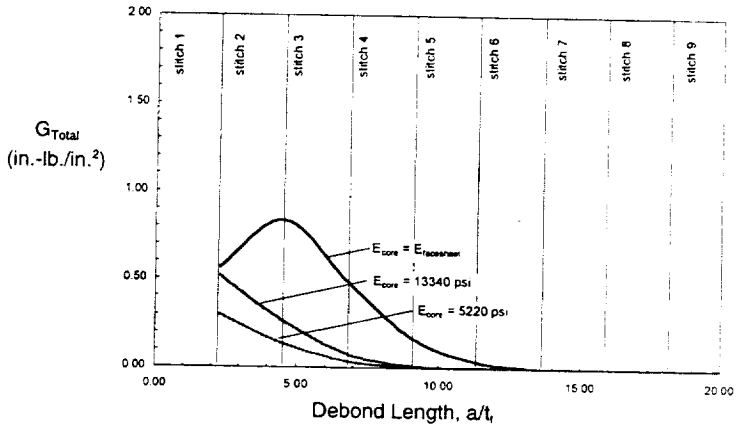

(b) Average stitch values

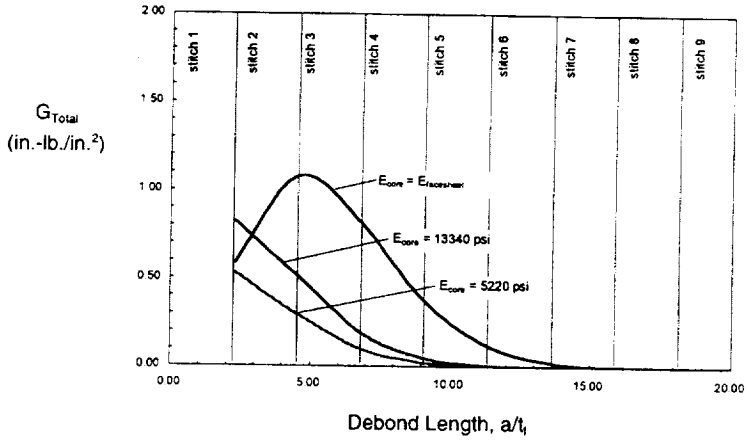

(c) Compliant stitch values

Figure 6. Strain energy release rate for configuration with 4 stitches per inch.

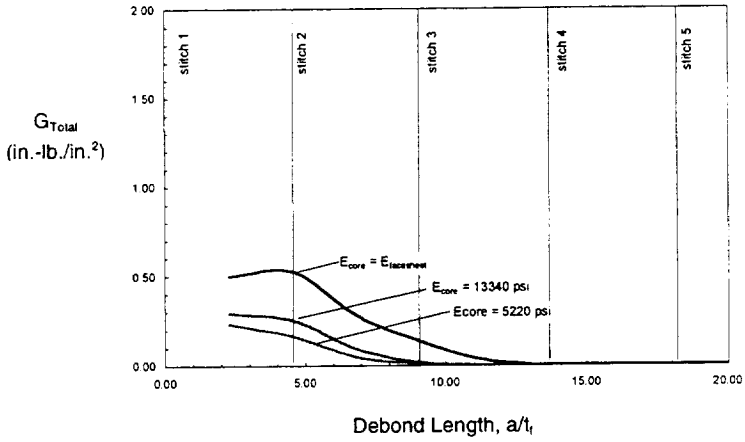

(a) Stiff stitch values

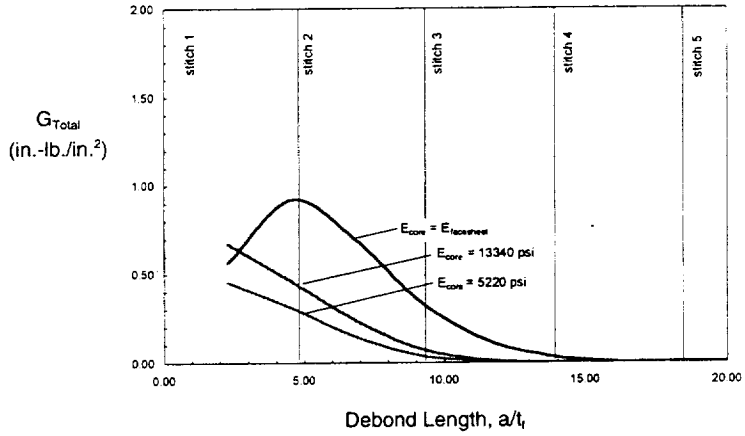

(b) Average stitch values

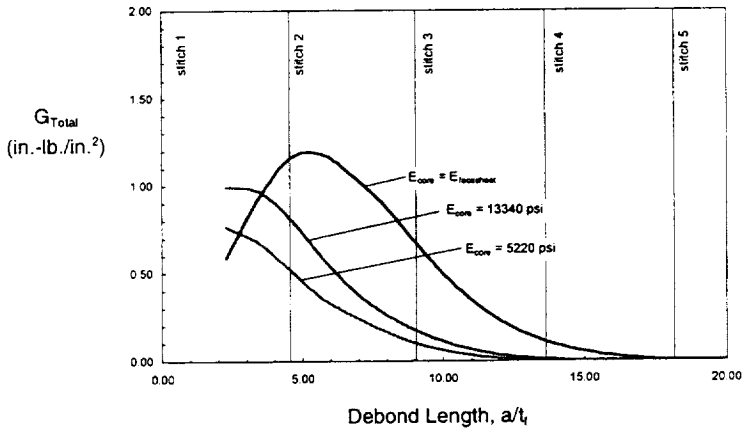

(c) Compliant stitch values

Figure 7. Strain energy release rate for configuration with 2 stitches per inch.

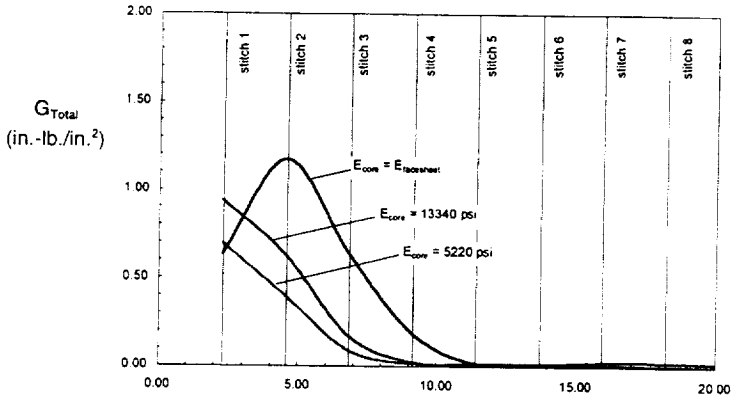

(a) Stiff stitch values

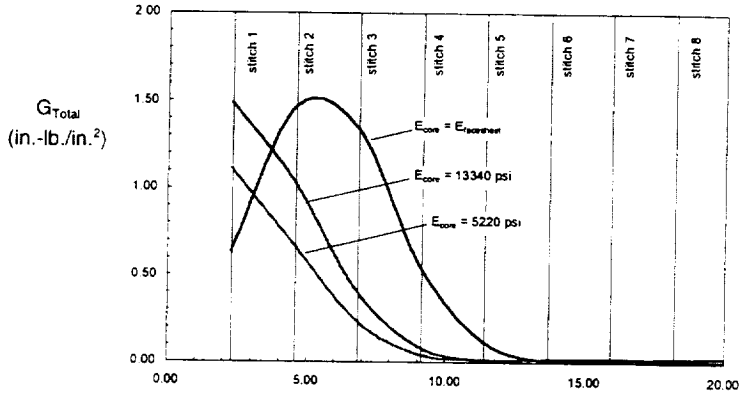

(b) Average stitch values

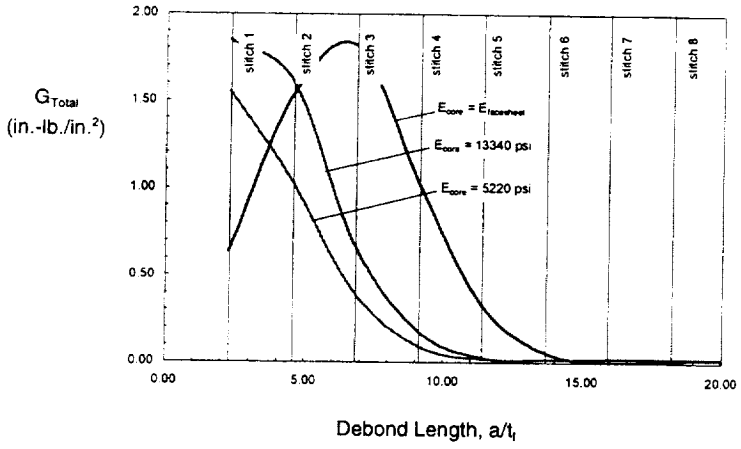

(c) Compliant stitch values

Figure 8. Strain energy release rate for configuration with 4 stitches per inch (no stitch under the loading point).

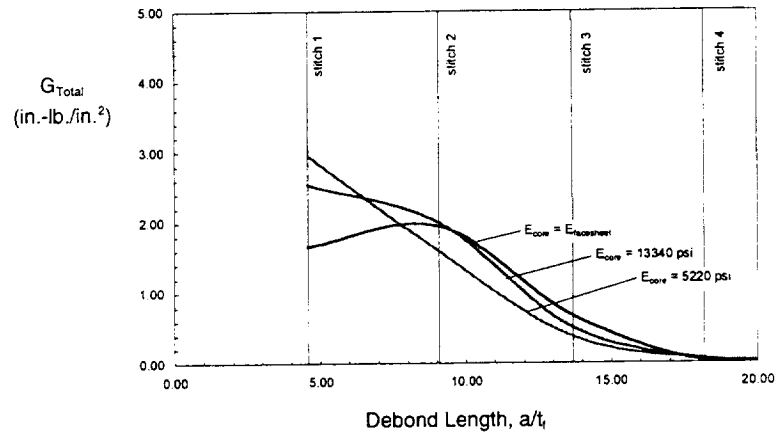

(a) Stiff stitch values

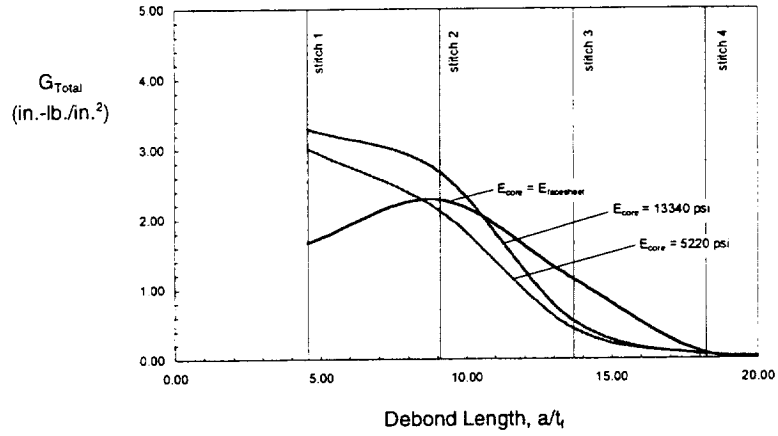

(b) Average stitch values

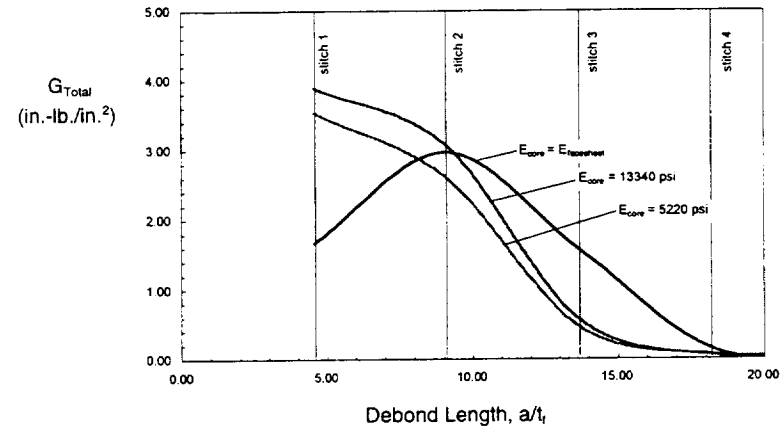

(c) Compliant stitch values

Figure 9. Strain energy release rate for configuration with 2 stitches per inch (no stitch under the loading point).